AIAA-93-0879
Application of High-Order Accurate Essentially Nonoscillatory Schemes to Two-Dimensional Compressible Viscous Flows

X. Zhong
Univ. of California
Los Angeles, CA

31st Aerospace Sciences Meeting & Exhibit
January 11-14, 1993 / Reno, NV

APPLICATION OF HIGH-ORDER ACCURATE ESSENTIALLY NONOSCILLATORY SCHEMES TO TWO-DIMENSIONAL COMPRESSIBLE VISCOUS FLOWS

Xiaolin Zhong *
Mechanical, Aerospace and Nuclear Engineering Department
University of California, Los Angeles, CA 90024

Abstract

The complexity of hypersonic flow requires efficient and accurate numerical methods for flow-field prediction. Since the current numerical methods for hypersonic flow computations are usually only second order accurate, we apply the essentially nonoscillatory (ENO) schemes, which are uniformly high order accurate to two-dimensional compressible viscous flow, with solid boundaries using body-fitted structured grids. Implicit methods are used to solved the Navier-Stokes equations by using the ENO schemes for the test cases of steady high-Reynolds-number viscous flows, which include supersonic boundary layer, shock/boundary-layer interaction flow, and type IV hypersonic shock-wave interfence heating problem. Results of the third order accurate ENO scheme for solving the Navier-Stokes equations have been obtained for the test cases. These results show that the 2-D ENO schemes are able to compute viscous flows with high resolution.

I. Introduction

The complexity of hypersonic flow requires efficient and accurate numerical methods for flow-field prediction. In numerical computations for viscous hypersonic flow, the presence of discontinuity surfaces of flow variables, such as shock waves, contact surfaces, and combustion fronts, makes it difficult to obtain high order accurate numerical solutions. An example of these flow problems is the shock-wave interference heating problem. It is a critical problem in the development of future hypersonic vehicles because the most intense local heating rates on the vehicle are expected to be on cowl lips caused by this shock-shock heating[1]. Therefore we need to accurately and efficiently predict these flow characteristics. But the shock-shock interference problem is a difficult problem for numerical computation because the strong shock waves and shear layers occur and interact with one and the other to form complicated flow patterns. High order accurate shock capturing numerical schemes are necessary to compute the flow structure.

*Assistant Professor, Member AIAA

In the neighborhood of the discontinuity surfaces of the flow variables, conventional methods based on central difference approximation yield oscillatory solutions. Upwind difference schemes have been developed to capture the shock waves and other discontinuity surfaces without oscillation. However, a straight forward extension of the first order upwind schemes to higher order accuracy leads to oscillatory solutions around the shock waves. The need of high resolution nonoscillatory numerical solutions has led to the development of total variation diminishing (TVD) schemes[2], which have been successfully used to compute practical flow problems using the Euler and Navier-Stokes equations. In order to prevent the total variation of the solutions from increasing, however, the TVD schemes are not uniformly higher order accurate. It is necessary for these schemes to reduce to first order accurate at local extrema of the solutions while maintain second order accuracy in other smooth regions.

In recent years, a class of essentially nonoscillatory (ENO) schemes, which are able to achieve uniformly high order accuracy, has been introduced by Harten, Engquest, Osher and Chakravarthy[3]. The ENO schemes present a hierarchy of uniformly high order accurate schemes which are generation of Godunov's scheme, its second order accurate MUSCL extension[4] to arbitrary order of accuracy. The ENO schemes attempt to avoid the growth of spurious oscillation in numerical solutions by piecewise polynomial interpolations based on adaptive stencil, which is chosen according to the local smoothness of the flow variables to avoid interpolation across discontinuities.

Because of uniformly high order accuracy of the ENO schemes, they are particularly appropriate for flow computations where uniformly high order accuracy are needed to compute flow with discontinuity fronts. One example of these flows is the hypersonic shock-wave interference heating problem. more over, they are also suitable to compute unsteady high-frequency flow physics. An example of their applications is the simulation of shock-wave turbulence interaction in a flow field with complicated geometries, which are not easily solved by the spectral methods.

Since their introduction, the ENO schemes have been applied successfully to solve many 1-D and 2-D Euler

Equations and Navier-Stokes equations. Recent applications can be found in Refs. [5, 6, 7, 8, 9]. For the 2-D Euler equations, Casper extended the ENO schemes based on the finite volume approach to general 2-D curvilinear grids and has applied the ENO schemes to 2-D boundary value problems for the Euler equations. He obtained some promising results for two dimensional Euler equations with non-trivial geometries and solid wall by using the 2-D ENO schemes of up to 4th order accuracy.

However, the ENO schemes have not been applied to multidimensional compressible viscous flows with non trivial geometries and solid wall, which are of practical importance in aerospace applications, and the performance of the ENO schemes in the viscous boundary layer is still unknown. Therefore, the objective of this paper is to apply the high order ENO schemes to high-Reynolds-number viscous flows by using curvilinear grids and to evaluate the performance of the ENO schemes for these viscous flow computations.

In this paper, the ENO schemes are applied to the following test cases of viscous flows:

- Supersonic flow of Mach 2 over a boundary layer of flat plate. This case, which does not involve a shock wave in the boundary layer, is chosen to test the performance of the 2-D ENO schemes on smooth viscous flow fields.
- Shock/boundary-layer interaction problem. An external oblique shock incident upon a boundary layer on a flat plate is chosen to be strong enough to cause the boundary layer to separate from the surface and reattach downstream.
- Shock-wave interference heating on a 2-D cylindrical leading edge.

The results of viscous flow computations using the 2-D ENO schemes of different orders of accuracy are evaluated, especially the third order accurate ENO scheme, which is one order more accurate than most of the current methods. The results of the present computations are also compared with available experimental results and numerical results by using other numerical methods.

II. ENO Schemes for Navier-Stokes Equations

Navier-Stokes Equations

In the Cartesian coordinates, the two-dimensional Navier-Stokes equations can be written in the following conservation-law form:

$$\frac{\partial U}{\partial t} + \frac{\partial F}{\partial x} + \frac{\partial G}{\partial y} = 0 \tag{1}$$

where $U = [\rho, \rho u, \rho v, e]^T$, $F = F_e + F_v$, and $G = G_e + G_v$. F_e and G_e are the inviscid flux terms and F_v and G_v are the viscous flux terms, i.e.,

$$F_e = \begin{Bmatrix} \rho u \\ \rho u^2 + p \\ \rho uv \\ eu + pu \end{Bmatrix}, \quad G_e = \begin{Bmatrix} \rho v \\ \rho uv \\ \rho v^2 + p \\ ev + pv \end{Bmatrix} \tag{2}$$

and

$$F_v = \begin{Bmatrix} 0 \\ \sigma_{11} \\ \sigma_{12} \\ \sigma_{11}u + \sigma_{12}v + q_1 \end{Bmatrix} \tag{3}$$

$$G_v = \begin{Bmatrix} 0 \\ \sigma_{21} \\ \sigma_{22} \\ \sigma_{22}v + \sigma_{21}u + q_2 \end{Bmatrix} \tag{4}$$

In the equations above, e denotes the total energy per unit volume ($e = CvT + (u^2+v^2)/2$); the gas is assumed to be perfect gas with $\gamma = 1.4$. Using tensor notation the viscous stress and heat flux are given by

$$\sigma_{ij} = -\mu \left[\frac{\partial u_i}{\partial x_j} + \frac{\partial u_j}{\partial x_i} - \frac{2}{3}\delta_{ij} \frac{\partial u_k}{\partial x_k} \right] \tag{5}$$

$$q_i = -\kappa \frac{\partial T}{\partial x_i} \tag{6}$$

where μ and κ are computed by using the Sutherland's law and a constant Prandtl number assumption ($Pr = 0.72$).

The Cartesian coordinates are used to demonstrate the numerical methods used in the present paper. In the finite volume approach, the integral form of the governing equations is used. For the grid cell (i, j), which represents a rectangle $(x_{i-\frac{1}{2}}, x_{i+\frac{1}{2}}) \times (y_{j-\frac{1}{2}}, y_{j+\frac{1}{2}})$, the intergal form of the conservation equations can be obtained by integrating Eq. (1) with respect to x and y over the cell,

$$\frac{\partial \overline{\overline{U}}_{ij}}{\partial t} + \frac{1}{A_{ij}} \left[\tilde{F}_{i+\frac{1}{2},j} - \tilde{F}_{i-\frac{1}{2},j} + \tilde{G}_{i,j+\frac{1}{2}} - \tilde{G}_{i,j-\frac{1}{2}} \right] = 0 \tag{7}$$

where $A_{ij} = \Delta x_i \times \Delta y_j$ is the area of the cell and $\overline{\overline{U}}_{ij}$ is the cell average of U,

$$\overline{\overline{U}}_{ij} = \frac{1}{A_{ij}} \int_{x_{i-\frac{1}{2}}}^{x_{i+\frac{1}{2}}} \int_{y_{j-\frac{1}{2}}}^{y_{j+\frac{1}{2}}} U(x, y, t)\, dy\, dx \tag{8}$$

$\tilde{F}_{i+\frac{1}{2},j}$ and $\tilde{G}_{i,j+\frac{1}{2}}$ are the cell surface integrals of the fluxes given by

$$\tilde{F}_{i+\frac{1}{2},j} = \int_{y_{j-\frac{1}{2}}}^{y_{j+\frac{1}{2}}} F(x_{i+\frac{1}{2}}, y, t)\, dy \tag{9}$$

$$\tilde{G}_{i,j+\frac{1}{2}} = \int_{x_{i-\frac{1}{2}}}^{x_{i+\frac{1}{2}}} G(x, y_{j+\frac{1}{2}}, t)\, dx \tag{10}$$

Numerical methods in solving Eq. (7) involve two procedures: formulating the numerical approximation of surface flux integrals and then using a time stepping scheme to solve Eq. (7), which reduces to a system of ordinary differential equations.

Surface Flux Integrals Approximation

The first step is to formulate the numerical approximation for surface flux integrals $\tilde{F}_{i+\frac{1}{2},j}$ and $\tilde{G}_{i,j+\frac{1}{2}}$ based on the cell average values $\overline{\overline{U}}_{ij}$. For $\tilde{F}_{i+\frac{1}{2},j}$, the surface integrals in Eq. (9) are numerically evaluated by using the Gaussian quadrature. For the first and second order accurate schemes, one point Gaussian quadrature is used; for second and third order accurate schemes, two-point Gaussian quadrature is used, etc. In order to compute the Gaussian quadrature, we need to evaluate the flux term $F = F_e + Fv$ at Gaussian quadrature points, where the viscous and the Euler flux terms are computed by using differently methods. F_v is evaluated by using central difference approximation, while F_e is evaluated by using a upwind difference scheme in order to capture shock waves without oscillation.

In the finite volume formulation, however, only the cell-averaged values of flow variables $\overline{\overline{U}}_{ij}$ are obtained in solving the conservations. Therefore, the first step in evaluating the inviscid fluxes is to reconstruct from $\overline{\overline{U}}_{ij}$ the point values of flow variables, U_L and U_R, on the left and right sides of the cell interface $S_{i+\frac{1}{2}}$. The ENO schemes use adaptive piecewise polynomial interpolation to reconstruct the point values of variables U_L and U_R. Since a fixed stencil high-order polynomial interpolation leads to oscillatory interpolation across discontinuity of the variables, the ENO schemes choose the "smoothest" interpolation stencils to reconstruct the point value of flow variables, thus avoid interpolation across discontinuities so that essential nonoscillatory schemes can be achieved with uniformly high order accuracy.

Following the reconstruction step, the flux F_e is computed by using an upwind approximation formula based on the approximate values of U_L and U_R, There are many available unwind schemes to compute inviscid flux. The present studies use the Roe approximate Riemann solver[10] as follows:

$$F_e(x_{i+\frac{1}{2}}, y, t) = \frac{1}{2}[F(U_L) + F(U_R)] - \frac{1}{2}|A|(U_R - U_L) \quad (11)$$

where $|A|$, which is evaluated based on the Roe average of flow variables U_L and U_R, is derived from the diagonalized form of the Jacobian matrix of F_e with all the eigenvalues replaced by their corresponding absolute values. It has been shown that the Roe scheme show may violate the entropy condition when the magnitude of an eigenvalue of matrix $|A|$ is very small and may create nonphysical expansion shock in the solution. Following Harten[2], the eigenvalue of $|A|$ is modified to be

$$\lambda = \frac{\lambda^2 + 4\epsilon^2}{4\epsilon^2} \quad \text{for} |\lambda| < 2\epsilon \quad (12)$$

where ϵ is chosen to be

$$\epsilon = \tilde{\epsilon}(u_n + c) \quad (13)$$

where u_n is the normal velocity on cell interface and c is the speed of sound. In the computations of the cases in this paper, only the case of shock-on-shock interference heating problem needs modification with $\tilde{\epsilon} = 0.2$.

Implicit Time-Stepping Scheme

After the approximate formulation of the flux intergals has been obtained, Eq. (7) reduces to a system of ordinary differential equations, which can be solved by using a time stepping scheme. For unsteady flow computations, we use explicit time accurate methods in the ENO schemes to compute the flow problems. In this paper, Eq. (7) is integrated by using the TVD Runge-Kutta time stepping schemes of Shu and Osher[11] to obtain the sell averaged variables $\overline{\overline{U}}_{ij}$ at the next time step.

On the other hand, for high-Reynolds-number viscous flow simulation, the grid size across the boundary layer near body surfaces is so small that explicit methods use prohibitively long computer time to reach steady state solutions because the time step has to be very small to satisfy stability conditions. Therefore, Eq. (7) is integrated by the implicit line Gauss-Seidel relaxation methods described by MacCormack[12] so that large CFL number can be used to rearch fast convergence for steady state problems. The method has been shown to be very robust and has been applied to 3-D computations and other hypersonic flow computations. We use the implicit equations in the delta form so that in the implicit part of the equations we can use the Steger-Warming flux splitting method, which is fast convergence for implicit methods, without having effects on the accuracy of steady state solutions.

For steady state problems, whether the ENO schemes are able to obtain steady state solutions have been questioned because the residual of the computations using the ENO schemes approaches a finite values instead of machine zero. The finite residual is caused by the unsteady adaptive interpolation procedure used in the ENO schemes. Nevertheless, our computational results show that the numerical computations can be considered to reach steady state solutions after the residual reaches a fixed pattern as time step increases.

1-D ENO Reconstruction

The ENO schemes have been documented extensively in the literature[3, 7]. The ENO interpolation used in this paper is briefly review below, more details can be found in the references cited above. The ENO reconstruction for a scalar function is considered herein, the extension to the Euler equations which is a system of equations is straight forward[3].

We want to evaluate the point value of $w(x)$ of a piecewise smooth function w from its cell average $\overline{w}_i$,

$$\overline{w}_i = \frac{1}{h_i}\int_{x_{i-\frac{1}{2}}}^{x_{i+\frac{1}{2}}} w(\xi)d\xi \tag{14}$$

where $h_i = x_{i+\frac{1}{2}} - x_{i-\frac{1}{2}}$. Given the cell average $\overline{w}_i$, we can immediately obtain the point value of the primitive function $W(x)$ $(= \int_{x_0}^{x} w(\xi)d\xi)$ as

$$W_{i+\frac{1}{2}} \equiv W(x_{i+\frac{1}{2}}) = \sum_{i=i0}^{i} \overline{w}_i h_i \tag{15}$$

Since

$$w(x) \equiv \frac{d}{dx}W(x) \ , \tag{16}$$

we obtain a piecewise polynomial interpolation function $H_m(x;W)$ of degree m by interpolating the point values of $W_{i+\frac{1}{2}}$ given by Eq. (15), and then obtain a pointwise approximation to $w(x)$ by

$$R(x;\overline{w}) = \frac{d}{dx}H_m(x;W) \tag{17}$$

where $R(x;\overline{w})$ denotes the reconstruction polynomial.

For cell $[x_{i-\frac{1}{2}}, x_{i-\frac{1}{2}}]$, we take $H_m(x;W)$ to be the mth-degree polynomial that interpolates the values of $W_{i+\frac{1}{2}}$ at $m+1$ successive points $x_{j+\frac{1}{2}}$, $j_m \le j \le j_m + m$ which include $x_{i-\frac{1}{2}}$ and $x_{i+\frac{1}{2}}$. Since there are m different choices of j_m, the interpolation stencil is not unique. The ENO schemes choose a stencil for $[x_{i-\frac{1}{2}}, x_{i-\frac{1}{2}}]$ such that $H_m(x;W)$ is "smoothest", which is extracted from a table of divided differences of $W(x)$. After an interpolation stencil has been chosen for every cell, the same divided difference table is used to compute the point value of w by using the Newton's divided difference formula for polynomial interpolation.

The use of adaptive interpolation stencils is the main contribution of the ENO schemes for high resolution computation across discontinuity surfaces. However, in smooth regions of the flow filed, the chattering stencils used in the ENO schemes can lead to a loss of accuracy[13]. Shu[14] has demonstrated that this loss of accuracy can be avoided by biasing the selection of the stencils in the smooth part of the solutions. Shu's modified ENO schemes are also tested and used in this paper.

Arbitrary Accuracy 2-D ENO Reconstruction

The extension of the 1-D ENO reconstruction procedure to the arbitrary accurate 2-D ENO reconstruction via primitive function is documented by Casper[7]. The implementation of 2-D ENO reconstruction is a composition of two applications of one-dimensional reconstructions in both x and y direction. The two-dimensional cell average $\overline{\overline{w}}_{ij}$ is

$$\begin{aligned}\overline{\overline{w}}_{ij} &= \frac{1}{\Delta x_i \Delta y_j}\int_{x_{i-\frac{1}{2}}}^{x_{i+\frac{1}{2}}}\int_{y_{j-\frac{1}{2}}}^{y_{j+\frac{1}{2}}} w(x,y)\,dy\,dx \\ &= \frac{1}{\Delta x_i}\int_{x_{i-\frac{1}{2}}}^{x_{i+\frac{1}{2}}}\left[\frac{1}{\Delta y_j}\int_{y_{j-\frac{1}{2}}}^{y_{j+\frac{1}{2}}} w(x,y)\,dy\right]dx\end{aligned} \tag{18}$$

The equation above can be written as

$$\overline{\overline{w}}_{ij} = \frac{1}{\Delta x_i}\int_{x_{i-\frac{1}{2}}}^{x_{i+\frac{1}{2}}} \overline{w}_j(x)\,dx \tag{19}$$

where

$$\overline{w}_j(x) = \frac{1}{\Delta y_j}\int_{y_{j-\frac{1}{2}}}^{y_{j+\frac{1}{2}}} w(x,y)\,dy \tag{20}$$

where the new piecewise smooth function $\overline{w}_j(x)$ is the line average in y in the interval of $[y_{j-\frac{1}{2}}, y_{j+\frac{1}{2}}]$, of $w(x,y)$ for a given x.

According Eqs. (19) and (20), we can reconstruct the 2-D point value of $w(x,y)$ from cell averages in two steps. First, for each j, Eq. (20) shows that $\overline{\overline{w}}_{ij}$ *is the line average in x direction of one-dimensional* function $\overline{w}_j(x)$ in the cell $[x_{i-\frac{1}{2},j}, x_{i-\frac{1}{2},j}]$. Therefore, the one-dimensional ENO interpolation procedure described previously can be used in x direction to obtained the point wise value of $\overline{w}_j(x)$. Then, for a given x, Eq. (20) shows that $\overline{w}_j(x)$ is the line average in y direction of one-dimensional function $w(x,y)$. Similar one-dimensional ENO interpolation procedure is used in y direction to obtained the point wise value of $w(x,y)$ by adaptively interpolate the point wise values of $\overline{w}_j(x)$, which have been obtained in the first step. Arbitrary order of accuracy can be achieved by using this full two-dimensional ENO interpolation procedure.

It is noted that the procedure above is not the extension to two-dimensions by simply "overlapping" two one-dimensional stencils in each direction. Casper[7] has shown that this "Dimension by Dimension" 2-D ENO schemes can only achieve second order accuracy. Since the main motivation of using the ENO schemes in this paper is to perform high order accurate computations, we use the arbitrary high order two-dimensional ENO reconstruction. The arbitrary accuracy 2-D ENO reconstruction procedure of this paper is programmed in a way such that reconstruction procedure is about two times as expensive as the "dimension by dimension" reconstruction and requires about two times as much memory.

General Curvilinear Coordinates

The 2-D ENO schemes for solving the Navier-Stokes equations in this paper are based on structured body-fitted grids. The use of the structured grids makes the arbitrary order two-dimensional ENO reconstruction more efficient compared with unstructured grids. It is noted that the ENO schemes for the Euler equations have been extended to two- and three- dimensional geometries by using unstructured grids[6, 15, 16]. Though the structured grids are not as flexible, most of the viscous flow problems can be represented by the structure grids.

In the general curvilinear coordinates in the body-fitted grids, the conservation equations in Cartesian coordinates are transformed in the curvilinear coordinates (ξ, η) in conservation-law form. The ENO construction procedures are extended to (ξ, η) space similar to the procedures in the Cartesian coordinates described above. The details can be found in Ref. [7].

Boundary Conditions

No slip boundary condition is used on the the wall surface. The flow variables in the supersonic free stream are specified, and those in the outflow boundaries are computed by using zeroth order or linear extrapolation. For high order ENO interpolation, the adaptive interpolations stencil is chosen such that only interior flow variables are involved in the interpolations.

Viscous Flux Computation

For the Navier-Stokes equations, the evaluation of intergals of viscous flux on the cell interfaces requires the first order derivatives of velocity and temperature. These derivatives are evaluated by using the central difference approximations based on the point wise value of the flow variables at the centroid of the cell, which can be reconstructed by using the ENO reconstruction. At present stage of this research, these values for viscous computations are taken to be the cell averaged value which are second order accurate. On the other hand the inviscid fluxes are evaluated at arbitrary accuracy. Our next step is to modify the viscous schemes so that the scheme is arbitrary high order accurate for both inviscid and viscous flux computations.

III. Numerical Results

The performance of the 2-D ENO schemes in solving the two-dimensional Navier-Stokes equations is tested by computing three test cases discussed in the introduction section. The test cases are computed by using five different test runs of the ENO (or modified ENO) schemes with spatial accuracy ranging from first to third order accurate as follows:

1. First order ENO scheme, which reduces to the first order Roe scheme.
2. Second order ENO scheme.
3. Second order Shu's modified ENO scheme.
4. Third order ENO scheme.
5. Third order Shu's modified ENO scheme.

The results of these test runs are compared with one and the other to evaluate the effect of increasing order of accuracy in the ENO schemes.

Supersonic Boundary Layer

The first test case, which does not involve a shock wave in the flow field and is chosen to test the performance of the 2-D ENO schemes on smooth viscous flow fields, is supersonic laminar flow over a flat plate. The free stream flow conditions are: $M_\infty = 2.0$, $Re_\infty/L = 1.65 \times 10^6/m$, $T_\infty = T_{wall} = 221.6K$ and $L = 1.83m$. The results of the two-dimensional ENO schemes for the Navier-Stokes equations are compared with the results of boundary layer computations which are taken from Ref. [17].

A set of coarse 20×20 grids (above the plate surface) which are uniformly spaced in both x and y directions, is used to compute the boundary-layer flow. The velocity and temperature profiles across the boundary layer at $x = 0.915m$ are plotted to compare with the results obtained from the boundary layer code.

Figs. 1 to 2 show the velocity profiles across the supersonic boundary layer at $x = 0.915m$ computed by the five test runs. Fig. 3 shows the corresponding temperature profiles. In general, these results show that as the order of accuracy of the ENO schemes increases, the accuracy of both the velocity and temperature profiles improves. The results of using Shu's modified ENO schemes shows improvement of accuracy compared with the corresponding ENO schemes without modification. On the other hand, the computations using the modified ENO schemes show more fluctuation in the convergence process compared with the ENO schemes.

The results of the first test case show that the ENO schemes are able to predict steady viscous flows in the boundary layer with high accuracy. The Shu's modified ENO schemes improve the accuracy of the ENO schemes in the boundary layer, but tend to be slightly more oscillatory. Overall, Shu's modified ENO schemes are preferred over the unmodified ENO schemes for viscous flow computations.

Shock-Wave/Boundary Layer Interaction

This test case, which is intended to evaluate the performance of the ENO schemes in viscous boundary

layer with steep gradients of the flow variables presense in the flow field, is the interaction of an oblique shock wave with a laminar boundary layer. Fig. 4, which is taken from [18], shows the flow field representing this interaction. The external oblique shock incident upon a boundary layer on a flat plate is chosen to be strong enough to cause the boundary layer to separate from the surface and reattach downstream.

The same problem has been studied experimentally by Hakkinen et. al.[19] at the following free stream flow conditions: $M_\infty = 2.0$, $Re_\infty = 2.96 \times 10^5$, and the incident shock wave is imposed such that its direction intersects the flat plate at 32.6 degrees. The Reynolds number is based on the reference length measured from the leading edge to the intersection point. The same problem has been studied extensively by many authors using various numerical methods[18, 20].

In the present studies, the five test runs are used to computed the flow field of shock/boundary-layer interaction using different grid resolutions. Only the results of the first order, the second and third order ENO schemes with Shu's modification are shown in this paper due to space limitation. The results presented here are computational results using a 102×144 grids above the plate surface. A set of uniformly spaced grids is used in x direction and an exponentially stretched grids are used in y direction. The implicit ENO scheme with Roe scheme without entropy correction are used in the computations. The CFD number for typical run is 5×10^5. Each run takes about 200 iteration until the solution converge to a fix pattern. For the grids in the present case, the first order implicit computation takes about 0.6 minute per time step in an IBM RISC600 workstation, while the second order ENO scheme takes about a factor 2 and the third order ENO scheme takes about a factor 3.5 CPU time per step.

Figs. 5 shows skin friction coefficient defined by $c_f = \tau/(\rho_\infty u_\infty^2/2)$. The numerical results are compared with experimental results of Hakkinen at. al.[19] and the numerical results of MacCormack[18]. The results show the improvement of accuracy as the order of the ENO schemes increases. The numerical results of the second and third ENO schemes are consistent with MacCormack's results which were computed with a coarse 32×32 grids and other numerical computations. These figures also show that the numerical results of the skin friction distribution obtained by high order ENO schemes are not very smooth in the separation region because the separation of the boundary layer and the modified ENO reconstruction is used.

Figs. 6 to 8 show the pressure contours of three test runs. From the figures, we can see that as the accuracy of the ENO schemes increases, the resolution of the captured shock becomes better. Again, the modified ENO schemes tend to be slightly more oscillatory in the interaction area.

Shock-Wave Interference Heating on a Cylinder

Fig. (9) shows a schematic of the flow field taken from Ref. [21]. The peak heating rates generated on the blunt leading edge by a shock incident on the bow shock in the stagnation region can be orders of magnitude greater than the stagnation value in the absence of the interaction. Since the intense shock waves, shear layer and viscous boundary layer that occur and interact with one and the other in a very small area, the problem is a very stiff one for numerically computation. Especially for type IV interaction, which shows most severe interference heating, it has been found that the flow field inherently unsteady which makes numerical computation more difficult.

Previous studies include experimental studies[22], theoretical studies, and numerical studies[23, 24, 21]. Most of the previous numerical studies have been limited to 2nd order accuracy. The results showed that accurate computation of heat transfer rate is crucially dependent on the shock resolution in the numerical solutions. Therefore, ENO schemes with higher than 2nd order accuracy can be very useful to capture the flow physics with high accuracy.

We choose the type IV shock wave interfence heating case to evaluate the performance of the high order ENO schemes in computing hypersonic flow with complex shock-shock and boundary layer interaction. The results of the ENO schemes are compared with the experimental results. The flow condition chosen to be one of the cases studied by Thareja et. al.[25]. The free stream flow above and below the imping shock wave are:

$M_\infty = 8.30$	$M_{1\infty} = 5.25$
$T_\infty = 111.56K$	$T_{wall} = 294.44K$
$p_\infty = 986.33N/m^2$	$\delta = 12.5°$
Cylinder Radius $= 1.5in.$	
$\beta_\infty = 0$	

where β_∞ is the free stream flow angle and δ is the flow deflection angle across the imping shock wave.

Since the main purpose of this paper is to compare the third order accurate ENO scheme with the first and second order schemes, a relative coarse 80×68 grids are used for this problem as a test case. Fig. 10 shows the computation grids used in the present studies. The implicit method is used with a CFL number of 50-100 to drive the iteration to a solutions to steady state with each run takes about 1000 iteration. The Roe scheme with entropy correction ($\epsilon = 0.2$) is used in the inviscid flux evaluation. The problem has been show experimentally and numerically to be marginal unsteady[21]. Our computations do show that the results will not converge to a relatively stable pattern. Therefore, the results showed in this paper are the re-

sults at a particular moment in this marginal unsteady flow.

On the other hand, for mesh cell located at the shock-shock interaction point in the present test case, there are not enough smooth grid points for high order ENO interpolation to be nonoscillatory. Similar one-dimensional cases exist when two one dimensional shock waves meet each other[3]. As a result, higher order polynomial interpolation may produce nonphysical negative pressure and density. Followed Harten et. al., the order of reconstruction will be reduced locally if the following condition is not met at a cell during the reconstruction,

$$\left|\frac{p-\overline{p}}{\overline{p}}\right| \leq 0.8 \tag{21}$$

and

$$\left|\frac{\rho-\overline{\rho}}{\overline{\rho}}\right| \leq 0.8 \tag{22}$$

where $\overline{p}$ and $\overline{\rho}$ are the cell average pressure and density, and p and ρ are point values obtained by ENO reconstruction within the same cell. The order reduction is done only in the local one or two cell points near the shock interaction point and does not affect the overall accuracy in the smooth region.

Figs. (11) to (13) show the Mach number contours of the solutions using the first, second, and third order accurate ENO schemes. These figures show that as the orders of the ENO schemes increase, the resolution of the solutions in the interaction area improves and the arbitrary accurate ENO schemes do capture the detailed flow physics better.

Figs. (14) and (15) show the comparison of surface heating rate and surface pressure with experimental measurement by Wieting and Holden[22]. These results are reanalyzed and published by Thareja et. al.[23]. They also compared these experimental results with their numerical results using finite element methods. Followed the treatment of Thareja et. al. the peak heating rate and surface pressure in our results are normalized by those of undisturbed stagnation values, $Q_0 = 41.43\text{Btu/ft}^2s$ and $p_0/p_\infty = 83.5$.

From the figures, we can see that the numerical results follow the same trend of the experimental results, though the location of peak heating rate is off by about 7 degrees. This may be due to the coarse 80×68 grids used for this problem and interaction region is not resolved with enough grid resolution. Meanwhile, the location of the peak heating rate is very sensitive to the location of the impinging shock. Our grids are not fine enough to locate the imping shock accurately. Further studies are needed to resolved this issue. Still the third order ENO scheme works quite well for the present test cases and are particular useful for this kind of hypersonic computations.

IV. Conclusions

The essentially nonoscillatory (ENO) schemes, which are uniformly high order accurate, have been applied to two-dimensional compressible viscous flow with solid boundaries using body-fitted structured grids. Implicit ENO schemes for solving the Navier-Stokes equations have been applied to test cases of steady high-Reynolds-number viscous flows. The test cases include supersonic boundary layer, shock/boundary-layer interaction flow, and type IV shock-wave interference heating on a cylindrical lead edge. Results of the ENO schemes of up to uniformly third order accuracy for solving the Navier-Stokes equations have been obtained for these test cases.

The following conclusions have been reached:

1. Steady state solutions of viscous flows can be obtained efficiently by using the implicit 2-D ENO schemes.

2. Higher order accurate ENO schemes lead to better accuracy in capturing the shock waves and resolving the boundary layers which are important for hypersonic flow computation.

Acknowledgements

This research was supported by AFOSR grant F49620-92-J-0090.

References

[1] National Research Council (U.S.). Committee on Hypersonic Technology for Military Application. Hypersonic technology for military application. Technical report, 1989.

[2] A. Harten. High resolution schemes for hyperbolic conservation laws. *J. of Comp. Phys.*, 49:357–393, 1983.

[3] A. Harten, B. Engquist, S. Osher, and S. Chakravarthy. Uniformly high order accurate essentially non-oscillatory schemes, III. *Journal of Computational Physics*, 71(2), August 1987.

[4] Bram van Leer. Towards the ultimate conservative difference scheme. V. a second-order sequel to Godunov's method. *Journal of Comp. Phys.*, 32, 1979.

[5] J. Y. Yang. Third order nonoscillatory schemes for the Euler equations. AIAA Paper 90-0110.

[6] T.J. Barth and P.O. Frederickson. Higher order solution of the euler equations on unstructured grids using quadratic reconstruction. AIAA Paper 90-0013, January 1990.

[7] J. Casper. *Essentially Non-Oscillatory Shock Capturing Schemes to Multi-Dimensional Systems of Conservation Laws.* PhD thesis, Old Dominion University, December 1990.

[8] Chi-Wang Shu, G. Erlebacher, T. A. Zang, D. Whitaker, and S. Osher. High-order ENO schemes applied to two- and three-dimensional compressible flow. Report 91-09, CAM, 1991. Department of Mathematics, University of California, Los Angeles.

[9] H. L. Atkins. High-order ENO methods for the unsteady compressible navier-stokes equations. AIAA Paper 91-1557.

[10] P. L. Roe. Approximate riemann solvers, parameter vectors and difference schemes. *Journal of Comp. Phys.*, 43:357–372, 1981.

[11] C. Shu and S. Osher. Efficient implementation of essentially non-oscillatory schemes. Contractor Report ICASE Report No. 87-33, NASA, May 1987.

[12] R. W. MacCormack. Current status of numerical solution of the Navier-Stokes equations. AIAA Paper 85-0032, AIAA, January 1985.

[13] A. M. Rogerson and E. Meiburg. A numerical study of the convergence properties of ENO schemes. *Journal of Scientific Computing*, 5:151–167, June 1990.

[14] Chi-Wang Shu. Numerical experiments on the accuracy of ENO and modified ENO schemes. *Journal of Scientific Computing*, 5:127–149, June 1990.

[15] S.R. Chakravarthy, K.-Y. Szema, and C.-L. Chen. A universe-series code for inviscid cfd with space shuttle applications using unstructured grids. AIAA Paper 91-3340.

[16] Ami Harten and Sukumar R. Chakravarthy. Multi-dimensional ENO schemes for general geometries. Report 91-16, CAM, August 1991. Department of Mathematics, University of California, Los Angeles.

[17] S. L. Lawrence, J. C. Tannehill, and D. S. Chausee. Upwind algorithm for the parabolized Navier-Stokes equations. *AIAA Journal*, 27(9), September 1989.

[18] R. W. MacCormack. A numerical method for solving the equations of compressible viscous flow. *AIAA Journal*, 20(9), September 1982.

[19] R. J. Hakkinen, I. Greber, L. Trilling, and S. S. Abarbanel. The interaction of an oblique shock wave with a laminar boundary layer. Memo 2-18-59W, NASA, 1959.

[20] Z. Wang and B. E. Richards. High resolution schemes for steady flow computation. *Journal of Computational Physics*, 97:53–72, 1991.

[21] D. Gaitonde and J.S. Shang. The performance of flux-split algorithms in high-speed viscous flows. AIAA Paper 92-0186.

[22] A. R. Wieting and M. S. Holden. Experimental shock-wave interference heating on a cylinder at mach 6 and 8. *AIAA Journal*, 27, 1989.

[23] R. R. Thareja et. al. A point implicit unstructured grid solver for the euler and navier-stokes equations. *International J. for Numerical Methods in Fluids*, 9:405–425, 1989.

[24] G. H. Klopfer and H. C. Yee. Viscous hypersonic shock-on-shock interaction on blunt cowl lips. AIAA Paper 88-0233.

[25] M.S. Holden and J.R. Moselle. Theoretical and experimental studies of the shock wave-boundary interaction on compression surfaces in hypersonic flow. Technical report arl 70-0002, Aerospace Research Lab, WPAFB, OH, January 1970.

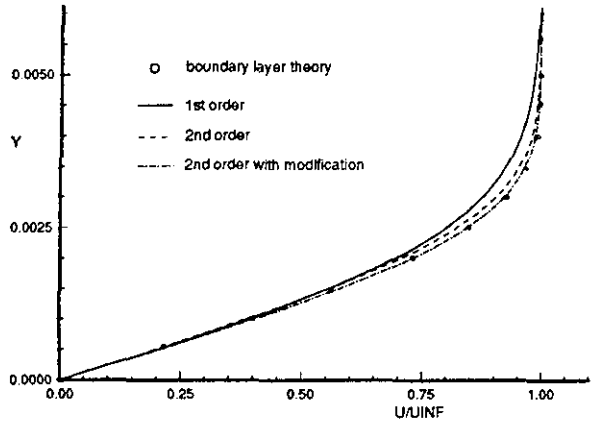

Figure 1: **Comparison of velocity profiles of the ENO schemes of first and second order and the boundary layer theory across supersonic boundary layer.**

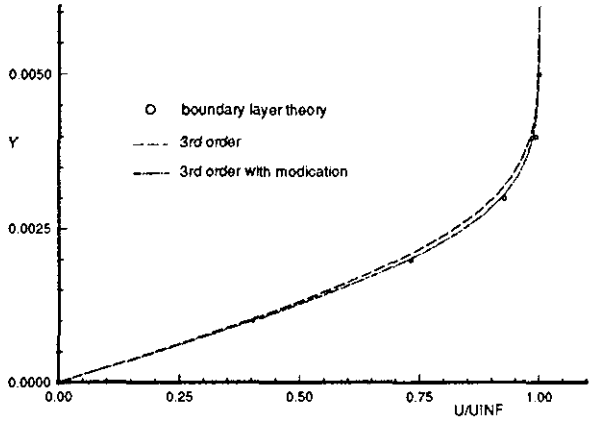

Figure 2: **Comparison of velocity profiles of the ENO schemes of third order and the boundary layer theory across supersonic boundary layer.**

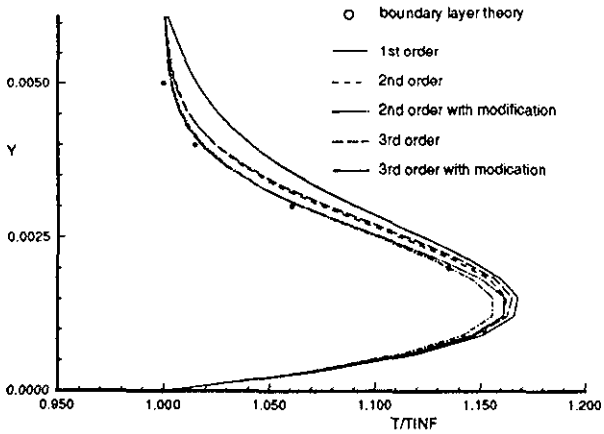

Figure 3: **Comparison of temperature profiles of the ENO schemes of 1st to third order and the boundary layer theory across supersonic boundary layer.**

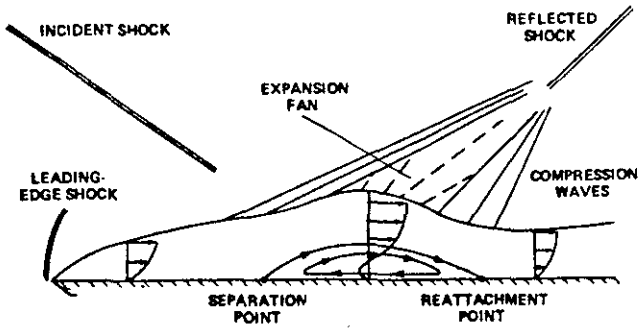

Figure 4: **Sketch of the flow field of shock/boundary-layer interaction.**

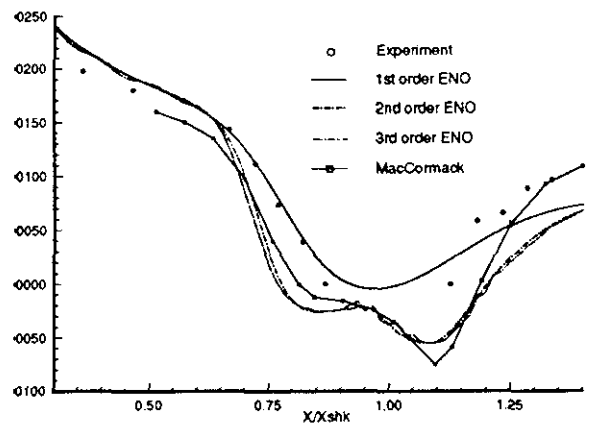

Figure 5: **Comparison of skin friction coefficient along plate surface for shock/boundary-layer interaction flow.**

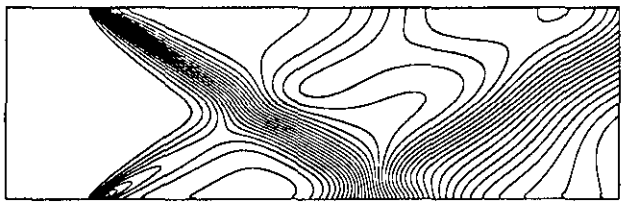

Figure 6: **Pressure contours obtained by using the first order ENO scheme.**

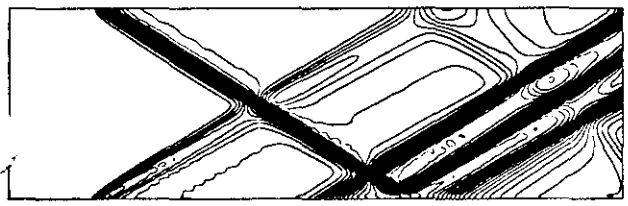

Figure 7: **Pressure contours obtained by using the second order ENO scheme with Shu's modification.**

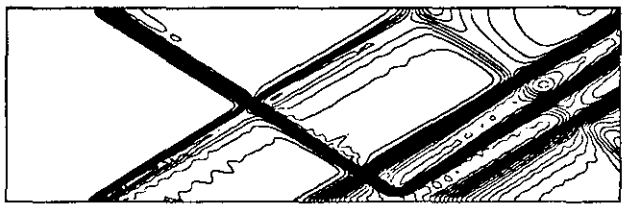

Figure 8: **Pressure contours obtained by using the third order ENO scheme with Shu's modification.**

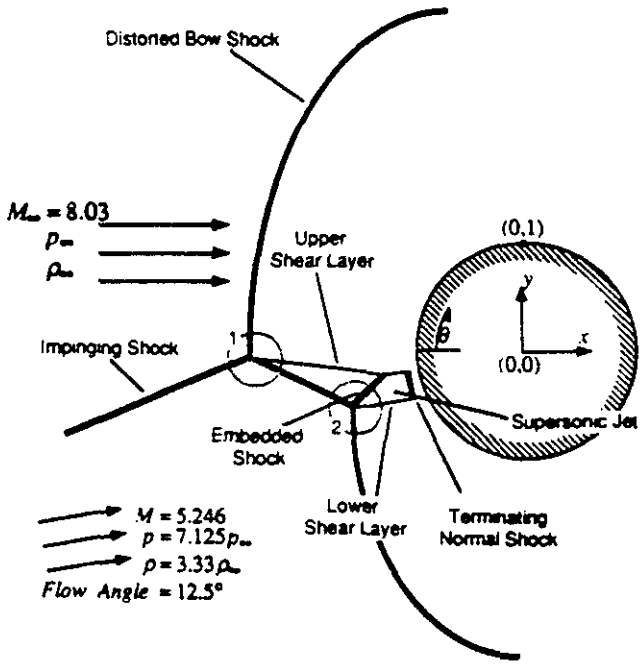

Figure 9: **Schematic of type IV shock-wave interference heating on a cylindrical leading edge.**

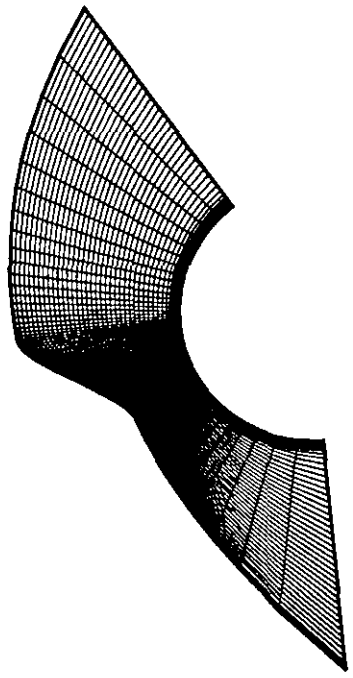

Figure 10: **Computational grids employed for type IV shock interference flow at $M_\infty = 8.03$**

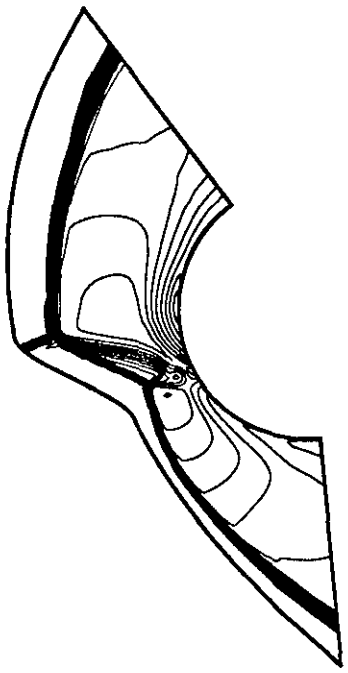

Figure 11: **Mach number contours for first order accurate ENO scheme for type IV shock interference flow at $M_\infty = 8.03$**

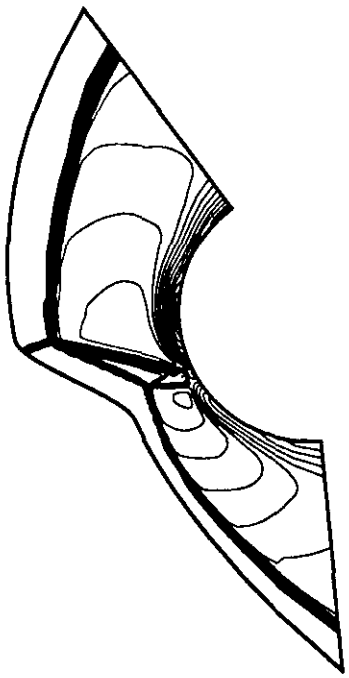

Figure 12: **Mach number contours for second order accurate ENO scheme for type IV shock interference flow at $M_\infty = 8.03$**

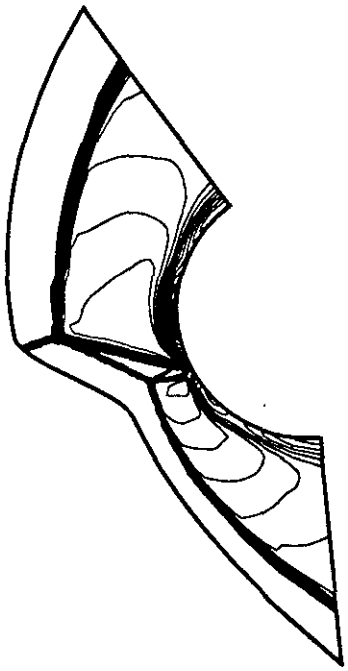

Figure 13: **Mach number contours for third order accurate ENO scheme for type IV shock interference flow at $M_\infty = 8.03$**

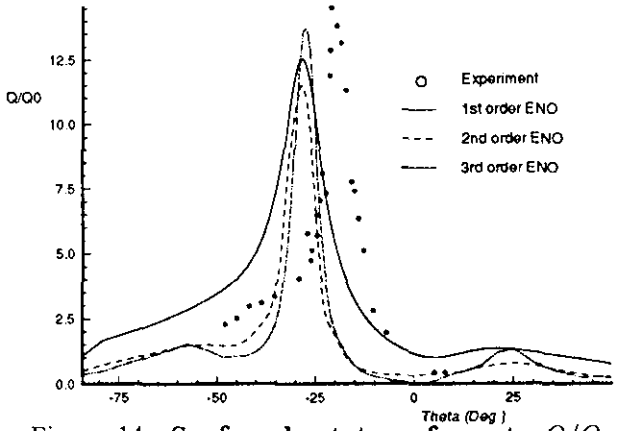

Figure 14: **Surface heat transfer rate Q/Q_0 for type IV shock interference flow at $M_\infty = 8.03$**

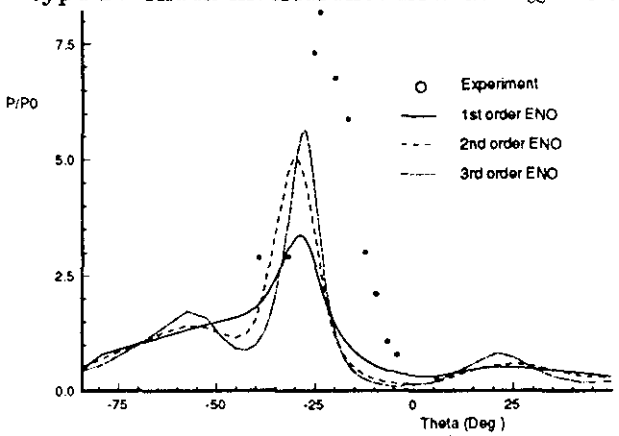

Figure 15: **Surface pressure p/p_0 for type IV shock interference flow at $M_\infty = 8.03$**